NANO LETTERS

pubs.acs.org/NanoLett Letter

The Scattering of Gold Nanorods Combined with Differential Uptake, Paving a New Detection Method for Macrophage Subtypes Using Flow Cytometery

Ruchira Chakraborty, Dorit Leshem-Lev, Ran Kornowski, and Dror Fixler*

Cite This: https://dx.doi.org/10.1021/acs.nanolett.0c03525 Read Online

ACCESS | Metrics & More | Article Recommendations | Supporting Information

ABSTRACT: The strategy of identification for M1 and M2 macrophages both *in vivo* and *in vitro* would help to predict the health condition of the individual. Here, we introduced a solution to this problem with the advantage of both the phagocytic nature of macrophages and the scattering effect of gold nanorods (GNRs). The internalized GNRs, relating to their extent of intake, caused a conspicuous scattering profile at the red channel in flow cytometry, overruling the contribution of the cellular side scatters. This internalization is solely governed by the surface chemistry of GNRs. The PAH-GNRs showed maximum intake potency followed by Cit-, PSS-, and PEG-GNRs. On a substantial note, PAH-GNRs lead to differential uptake between M1 and M2 cells, with three times higher intake in M2 cells over M1. This is the first report of employing the scattering of unlabeled GNRs to discriminate M1 and M2 cell types using a flow cytometer.

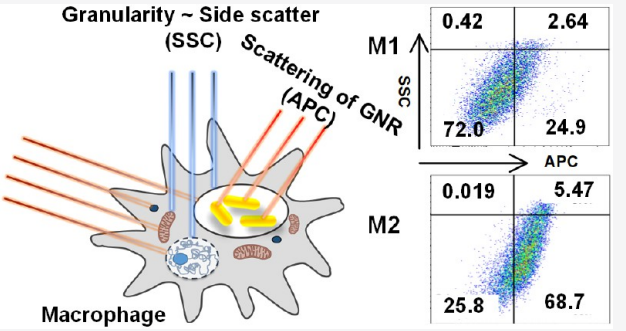

KEYWORDS: *scattering, gold nanorods, macrophages, M1/M2, flow cytometer, cellular uptake*

Macrophages are an integral part of our innate immune response.[1] The efficient phagocytic potency of macrophages defends us from a wide range of infectious and chronic inflammatory diseases.[2] Every solid organ has its macrophage niche, called tissue-resident macrophages.[3] The circulating blood monocytes also act as progenitors for macrophages.[4,5] Functional plasticity is one of the key characteristics of macrophages. The change in the inflammatory microenvironment under or during symptomatic phases governs the differentiation of macrophages into two major phenotypes: M1 (classically activated) and M2 (alternatively activated).[6−9] In the early stage of bacterial infection, M1 macrophages localize at the site of infection, but a long persistence of infection leads to M2 polarization. M2 population is reported in viral and parasitic infections.[10,11] In atherosclerosis, the M1 population is observed in vulnerable unstable plaques and M2 in stable, asymptomatic plaques.[12,13] M1 cells are found at the initial stage of the tumor, while, at the stage of metastasis, the population is shifted to M2 (often called TAM) type.[14,15] With this unique potency of the particular disease and stage-defined localization of M1/M2 macrophages, an assessment of the M1 vs M2 ratio could lead to a quick screening of the syndromes and would be a potential upcoming tool to predict the personalized treatment strategy. Until date, the detection of M1/M2 is done mostly *in vitro*, based on their specific surface markers (M1-CD80, CD86, CD68; M2- CD206, CD163) or, by expression of signature protein levels (IL-1β, IL-6, ferritin, inducible nitric oxide synthase (iNOS) for M1; TGF-β, IL-10, transferrin receptor 1, arginase for M2).[16] Here, we want to address the issue from the nanophotonics aspect to achieve a precise label-free approach that can even further translate to *in vivo* detection. The easily tunable versatile optical property, which comes with the advantage of biocompatibility, opens a wide range of biomedical applications for gold nanoparticles (GNPs).[17] By virtue of strong absorbance, GNPs have a promising future in biomedical diagnostics as a suitable contrast agent for cellular imaging, including two-photon photoluminescence microscopy, coherence tomography, photoacoustic tomography, and recently in diffusion reflection.[18−31] The high scattering potency of GNPs is utilized in optical imaging by dark field microscopy and confocal reflectance microscopy.[32,33] We chose gold nanorods (GNRs) for this study, as GNRs show an order of magnitude higher absorption and scattering coefficient relative to nanospheres of the same effective radius.[34]

Received: August 31, 2020
Revised: October 14, 2020

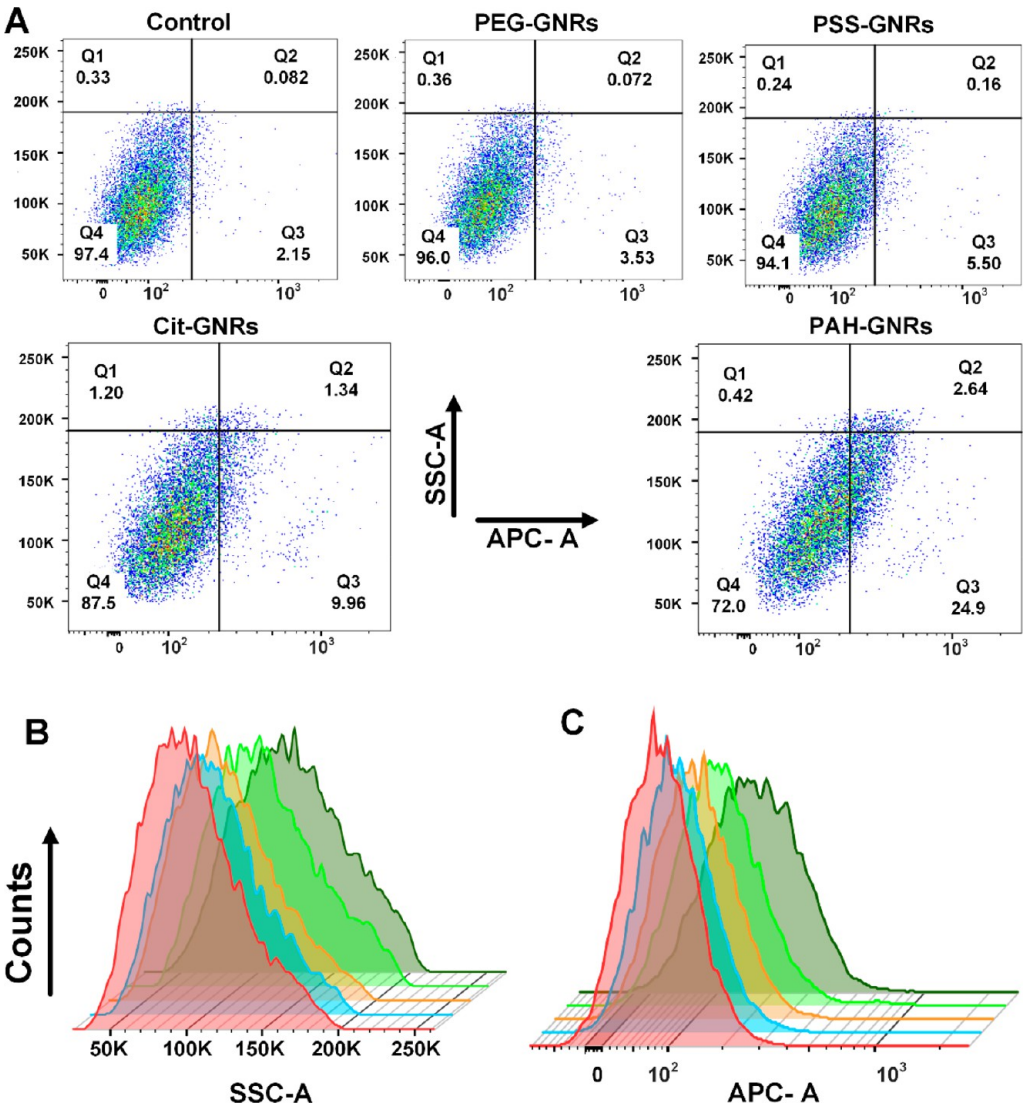

Figure 1. FCM analysis of M1-type macrophages (differentiated from THP1): (A) the dot plot of SSC vs APC intensities of unstained control cells and cells after GNR incubation. The histogram plot of (B) changes in SSC intensities and (C) APC intensities of cells with different GNR staining. Unstained control (red), PEG-GNRs (aqua), PSSGNRs (orange), Cit-GNRs (light green), and PAH-GNRs (dark green) stained M1 cells were shown in panels B and C.

Flow cytometry (FCM) is a popular method to monitor diverse physiological processes of a population of cells based on fluorescence labeling and scattering.[35] In our case, monitoring the change of side scatter (SSC) intensity could give us a hint about the internalization of GNRs, as the accumulation has a direct effect on intercellular granularity. Here we have an additional advantage to utilize the scattering of GNRs. As a normal flow cytometer is not equipped with any special arrangement for direct capture of the scattering of particles at or above our required wavelength, we simply utilized the red channel used for Allophycocyanin (APC) fluorescence. We hypothesized that, alongside SSC, the measure of scattered intensity for specific GNRs would lead us to a clearer view. This is the first attempt to relate the nanoparticle scattering as a measure of entrapped GNRs in macrophages.

Results. Our work intends to establish a scattering based distinction between M1 and M2 macrophages. The phagocytic tendency of macrophages ensures the intercellular accumulation of GNRs with ease. We postulated to get a well-defined pattern of cellular intake of GNRs with the aid of their strong scattering, which should be convenient to monitor with the flow cytometer. We approached this by different surface coatings of GNRs with biocompatible polymers: polyethylene glycol thiol (mPEG-SH, MW 5 kDa), poly(allylamine hydrochloride) (PAH, MW 17.5K g/mol), polystyrenesulfonate (PSS, MW 70K g/mol), and sodium citrate (Cit). Figure S1 showed the characteristics of the prepared GNRs. There are reports on the effect of the surface coating on the uptake of GNRs by undifferentiated macrophages. Here, we extended the study between M1/M2 subtypes on the influence of the surface layer in the cellular intake of GNRs. Before going to cellular intake studies, the dose-dependent cytotoxicity of GNRs was monitored for THP1 cells and its differentiated forms (showed in Figures S2−S5) along with the isolated macrophages from peripheral blood mononuclear cells (PBMCs) of healthy donors and with the further differentiated M1 and M2 forms (showed in Figures S6−S8). Bright-field microscopy stated the maintenance of the morphological integrity of THP1 cells with GNRs (Figures S9 and S10).

https://dx.doi.org/10.1021/acs.nanolett.0c03525
Nano Lett. XXXX, XXX, XXX−XXX

The FCM Study. The dot plot of SSC vs APC intensity represented the cellular scattering based on internalized GNRs. The control set represents the cell without any GNR exposures. The quadrants marked as Q1, Q2, Q3, and Q4 describe the population of cells with high SSC and low APC scattering; high SSC and high APC scattering; low SSC and high APC scattering; and low SSC and low APC scattering, respectively. Thus, the major population of GNRs unstained or negative cells will be at the Q4 quadrant, and the GNRs positive cells with high SSC and APC scattering would be found at the Q2. Simply, a shift of cellular population toward Q2 and Q3 signifies intracellular GNRs accumulation, and the extent of intake reflects the percentage increase of the respective cellular population. To verify our hypothesis, we first stained the THP1 cells and its PMA differentiated unpolarized macrophages with all four types of GNRs. The higher phagocytic property of macrophages over monocytes was highly evident in our FCM results (Figures S11 and S12). Besides, depending on their surface moiety, a particular propensity in cellular uptake of GNRs was observed, i.e., PEG-GNRs< PSS-GNRs < Cit-GNRs < PAH-GNRs.

We started to work with M1 and M2 types of macrophages differentiated from THP1, as we aimed to discriminate between the two cell types. The interaction with all four sets of GNRs with M1 cells maintained the same trend as unpolarized macrophages (Figure 1); i.e., PAH-GNRs showed the highest uptake, followed by Cit-GNRs, PSS-GNRs, and PEG-GNRs. However, except for PEG-GNRs, the uptake of each class of GNRs got an overall enhancement (Figure 1A). The Q2 quadrant showed distinctive changes with 2.0-, 16.53-, and 37.33-fold increases in M1 population for the consequent PSS-GNRs, Cit-GNRs, and PAH-GNRs staining. The variation in the Q3 quadrant was also prominent with 2.67-, 4.86-, and 10.84-fold increases in the M1 population for the corresponding PSS-GNRs, Cit-GNRs, and PAH-GNRs staining. The detailed analysis of the changes in SSC and APC intensities with different staining are shown in Figure 1B,C. The distinct shift in APC intensities indicates that the scattering of GNRs worked better in differentiating the GNR positive population compared to SSC scattering. Table 1 summarized the effect on median SSC and mean APC intensities in the presence of GNRs for M1-type cells.

Table 1. Change in Scattering Intensities in the Presence of GNRs for M1- and M2-Type Cells (Differentiated from THP1)

	median SSC-A intensity (au)		mean APC-A intensity (au)	
sample name	M1 cells	M2 cells	M1 cells	M2 cells
control	10.58×10^4	10.42×10^4	97.1	79.1
PEG-GNRs	10.78×10^4	10.63×10^4	103	85.3
PSS-GNRs	10.99×10^4	11.23×10^4	119	110
Cit-GNRs	11.96×10^4	12.76×10^4	180	168
PAH-GNRs	12.24×10^4	13.73×10^4	234	339

The profile of M2 cells after GNRs staining (Figure 2) followed the same order of cellular uptake; however, the PAH-GNRs had a noticeable uplift in APC scattering. Compared to M1 cells, the same amount of PAH-GNRs caused an extraordinary feature in SSC vs APC plots for M2 cells (Figure 2A). A shift of 34.18- and 43.16-fold of the M2 population was observed in the Q2 and Q3 quadrants with PAH-GNRs. The evident increase in the Q3 population gave an obvious indication of the massive cellular intake of PAH-GNRs in M2 compared to M1 cells. The PSS-GNRs and Cit-GNRs also showed a significant shift of M2 cells with a corresponding 5- and 31.87-fold increases in Q2 and 9.68- and 17.72-fold increases for Q3 quadrant. The Cit-GNRs also had significant changes between M1 and M2, but PAH-GNRs caused the higher and prominent difference. When we further look into the details of the change in the SSC and APC intensities (Figure 2B,C and Table 1), both, in SSC and APC channel PAH-GNRs, elicited distinct raise compared to the unstained control and all other types of GNRs.

We compared the effect of all four GNRs on the corresponding percentage increase of each SSC and APC intensities for both M1 and M2 cells (Figure 3). The percentage increase for each cell type was calculated over the SSC and APC values of respective unstained control cells. With PEG-GNRs staining, the extent of change in SSC remained the same for both M1 and M2 (Figure 3A). The distinguishing pattern between M1 and M2 cells in terms of SSC intensities appeared a bit with Cit-GNRs and was evident with PAH-GNRs. The scenario got a better understanding of the case of APC intensities (Figure 3B). Although PEG-GNRs and PSS-GNRs maintained the consistency, Cit-GNRs and PAH-GNRs staining made the difference. The 80.6% increase of APC intensities for M1 cells improved to 101.5% for M2 cells with Cit-GNRs. The PAH-GNRs scored the real contrast with a hike of 312.3% and 141.3% in APC scattering for the corresponding M2 and M1 cells. In short, PAH-GNRs lead to a differential uptake between M1 and M2, promoting nearly twice the uptake by M2 over M1 cells.

The fact of this differential uptake between M1 and M2 cells with PAH-GNRs staining firmly corroborates the results with the macrophages from PBMC (Figures S13 and S14). The scattering intensity in the APC channel inflated by 230.9% with PAH-GNR laden M2 macrophages (differentiated from PBMC macrophages, isolated from donor's blood), leaving behind the M1 cells with a 114.3% increase for the same. Notably, the effect of surface molecules maintained the same trends for both M1 and M2 macrophages from PMBC. We also investigated the effect of GNRs on other blood cell types, e.g., erythrocytes, lymphocytes, granulocytes, and monocytes, isolated from a healthy donor. Both the FCM (Figures S15−S18) and ICP analysis (Figure S19) verified a negligible effect of GNRs internalization for other blood cells and thus specified a selective clearance of GNRs by macrophages.

Thus, based on the scattering effect of internalized GNRs, FCM can differentiate between GNR laden and unstained macrophages, and a choice of the surface coating can lead to divergent patterns even among M1 and M2 cells. The change in FSC intensities also plays an important role in FCM. The decrease of FSC intensity showed (Figure S20) complete accordance with our expectation, i.e., PAH → Cit → PSS > PEG-GNRs. Additionally, the prominent decrease in FSC intensity for M2 cells compared to M1 revalidates our FCM analysis.

The time dependence on cellular internalization of PAH-GNRs showed that, for M2 cells, 24 h incubation caused the best uptake (Figure S21). As 24 h seems to be a prolonged incubation for an *in vitro* assay, we tried with low incubation times with a higher concentration of PAH-GNRs (100 μg/mL). Figures S22 and S23 showed a possible differentiation with 3 h of incubation only.

https://dx.doi.org/10.1021/acs.nanolett.0c03525
Nano Lett. XXXX, XXX, XXX−XXX

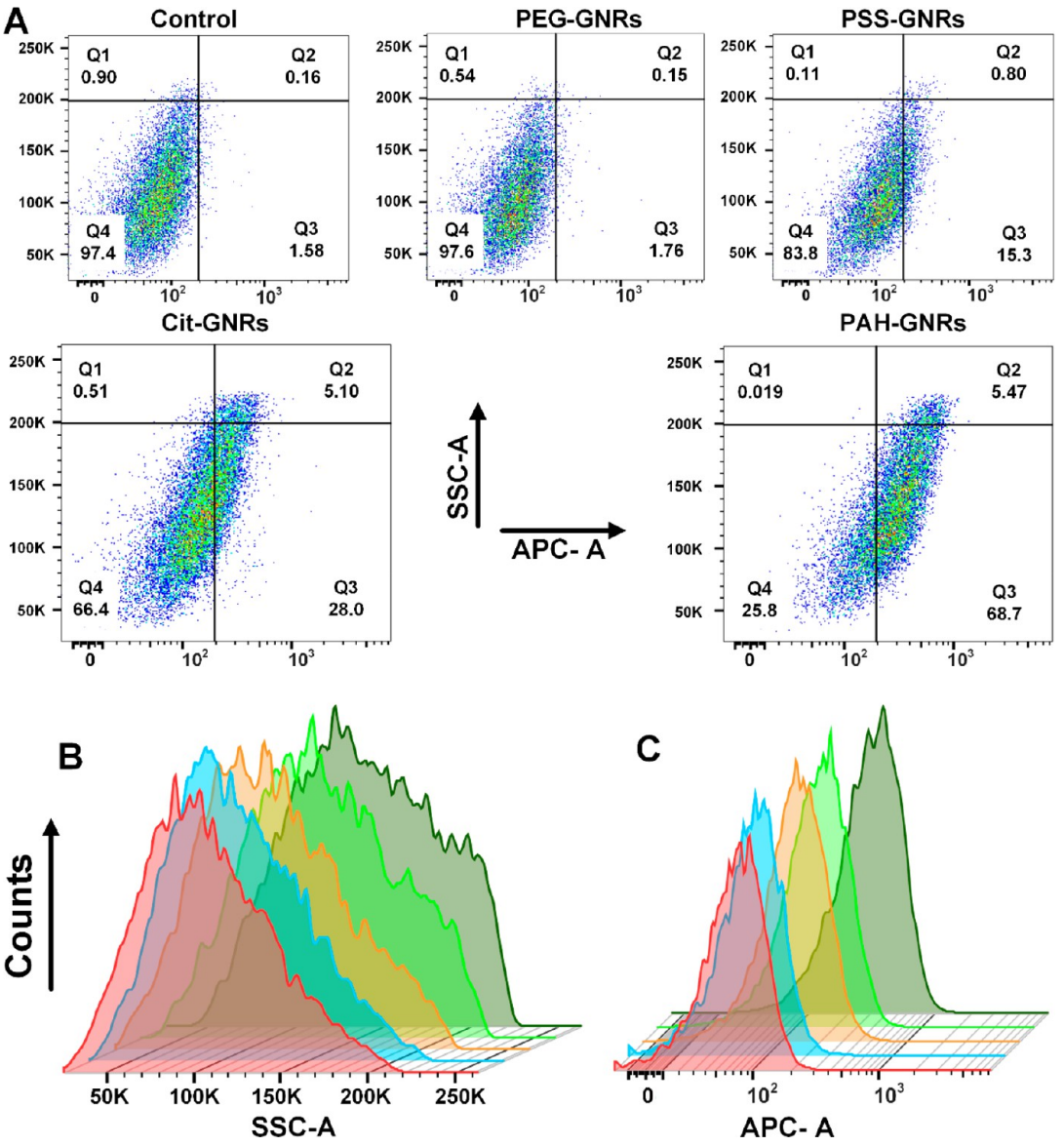

Figure 2. FCM analysis of M2-type macrophages (differentiated from THP1): (A) the dot plot of SSC vs APC intensities of unstained control cells and the cells after GNR incubation. The histogram plot of (B) changes in SSC intensities and (C) APC intensities of cells with different GNR staining. Unstained control (red), PEG-GNRs (aqua), PSSGNRs (orange), Cit-GNRs (light green), and PAH-GNRs (dark green) stained M2 cells were shown in panels B and C.

We also checked that the surface coating polymers (PEG, PSS, Cit, and PAH, 5 μM each) individually did not play any role in the respective cellular scattering in FCM studies (Figure S24). It implies that the coating caused a route of cellular entry, but enhancement of the scattering intensity in the SSC and APC channel was exclusively for the subsequent accumulation of GNRs itself.

Recently, in their work, Wu et al. showed that, apart from 488 nm, the use of red excitation lasers of 561 and 687 nm for the SSC measurements greatly enhanced the optical signal needed for the flow cytometry-based detection of intracellular gold nanospheres (GNS) and GNRs in triple-negative breast cancer cells (MDA-MB-231).[36] Zucker et al. also found the same with TiO_2−NPs and Ag-NPs for the epithelial cell line (ARPE-19).[37,38] The extent of intake of the TiO_2−NPs and Ag-NPs was correlated with the corresponding increase in SSC intensity and further confirmed with dark-field microscopy. The enhancement in signal intensity of SSC with the use of a red excitation source was also documented for Ag-NPs.[38] However, the contribution of scattering from either TiO_2−NP or GNS/GNR was not taken into account in the report. The novelty of our work counts on the measure of scattering from the ingested GNRs in the APC channel, together with the changes in SSC.

A Measure of the Intercellular Gold Concentration. The FCM studies so far indicated differential uptake of GNRs. However, to get the exact measure of internalized GNRs, we performed inductively coupled plasma (ICP) analysis (Figure 3C). The trend of internalization of GNRs followed the same as we got from FCM studies with PEG-GNRs at the lowest and PAH-GNRs at the highest grade. Most importantly, the PAH-GNRs was significantly higher than PEG-, PSS-, and Cit-GNRs for both cell types differentiated from THP1. The reason for getting a dramatic profile with PAH-GNRs in FCM studies now has a suitable explanation with the outcome of ICP results. Moreover, the overall higher accumulation of

https://dx.doi.org/10.1021/acs.nanolett.0c03525
Nano Lett. XXXX, XXX, XXX−XXX

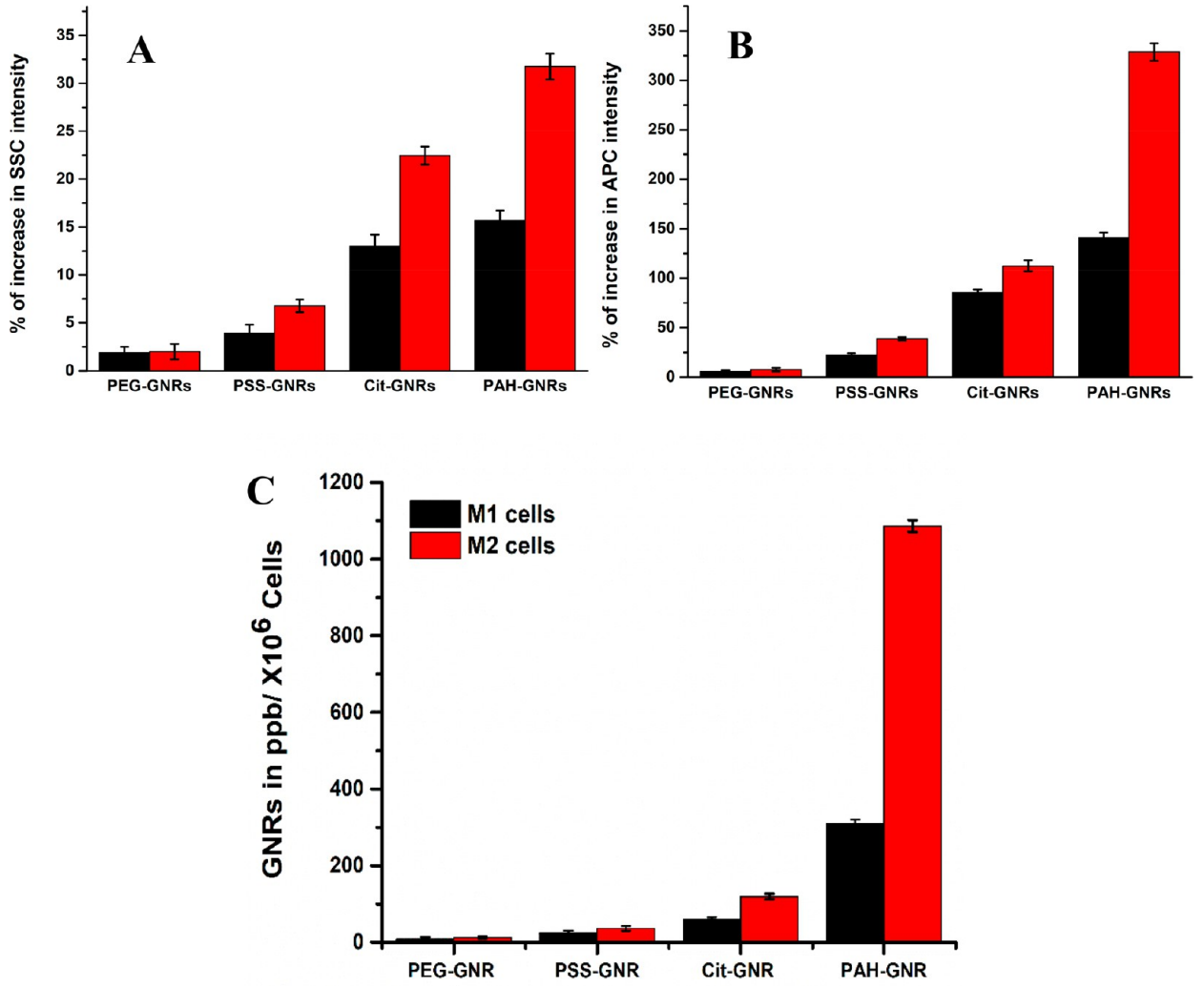

Figure 3. Comparison of GNR intake by M1 and M2 cells (differentiated from THP1). (A) The percentage increase in SSC and (B) APC intensities for different GNR staining. The calculation was made concerning the relative intensity of unstained control cells as the baseline. The black-colored bars represented M1-type cells, and the red-colored ones denoted M2-type cells. (C) The measure of the intercellular gold concentration of M1 and M2 cells, 24 h after their GNR intake, by ICP.

GNRs in M2 over M1 cells also supported the result from FCM. The discrimination between M1 and M2 cell types became evident with PAH-GNRs. The amount of internalization of PAH-GNRs was three times that in the case of M2 cells over M1 for the both THP1 and PBMC differentiated macrophages (Figure S25). This value had a good correlation with the data from the FCM result, where we got almost 2.2 and 2.0 times higher uptake of PAH-GNRs in M2 cells compared to M1 for corresponding macrophages from THP1 and PBMC. Overall, the ICP studies well documented our proof of concept.

Few groups worked on the uptake of GNPs by macrophages and other cells. The cellular uptake of nanoparticles was improved by PAH, PSS, and PAA coating or by the conjugation of BSA (bovine serum albumin) or aptamer.[33,39,40] The effect of size, shape, and AR of the particles was also discussed.[41,42] Shape-dependent cellular uptake of GNRs was found in MCF-7 cells, and with a similar surface coat, the higher AR had a lower intake.[42] Reports supported our result of ICP as PAH-GNRs showed a greater degree of cellular uptake over other particles. Alkilany et al. found 2320 ± 140, 270 ± 20, and 45 ± 6 GNRs of 4.1 AR per human colon carcinoma (HT-29) cells with the respective PAH, PAA, and CTAB coatings.[33] In an article by Zhu et al., the GNRs of around 3.0 AR showed a higher intake of PSS over PEG coating in the ICP studies for U-87 MG and PC-3 cells. These studies showed complete accordance with our data from ICP.[43] Further, lower accumulation of PAH-GNRs in the presence of caveolae and clathrin-mediated endocytosis inhibitors established the endocytic entry of GNRs in cells (Figure S26). This endocytosis is further confirmed by TEM images.

Envision of the GNRs Intake in M1/M2 Cells. Finally, the internalized PAH-GNRs were visualized through Cryo-TEM imaging. The previous results of ICP and FCM studies confirmed the highest intake of PAH-GNRs in macrophages. So, for TEM imaging, we only used PAH-GNRs staining. Figure 4 and Figure 5, respectively, showed the PAH-GNRs laden M1 and M2 cells. The cellular integrity remained unaltered with the PAH-GNRs exposure for both cell types. The presence of a prominent mitochondrion, well-defined nucleus, and Golgi all together indicated the innocuous nature of PAH-GNRs to the cells. A section of PAH-GNRs treated M1 cells is presented in Figure 4A. The area of GNRs

https://dx.doi.org/10.1021/acs.nanolett.0c03525
Nano Lett. XXXX, XXX, XXX−XXX

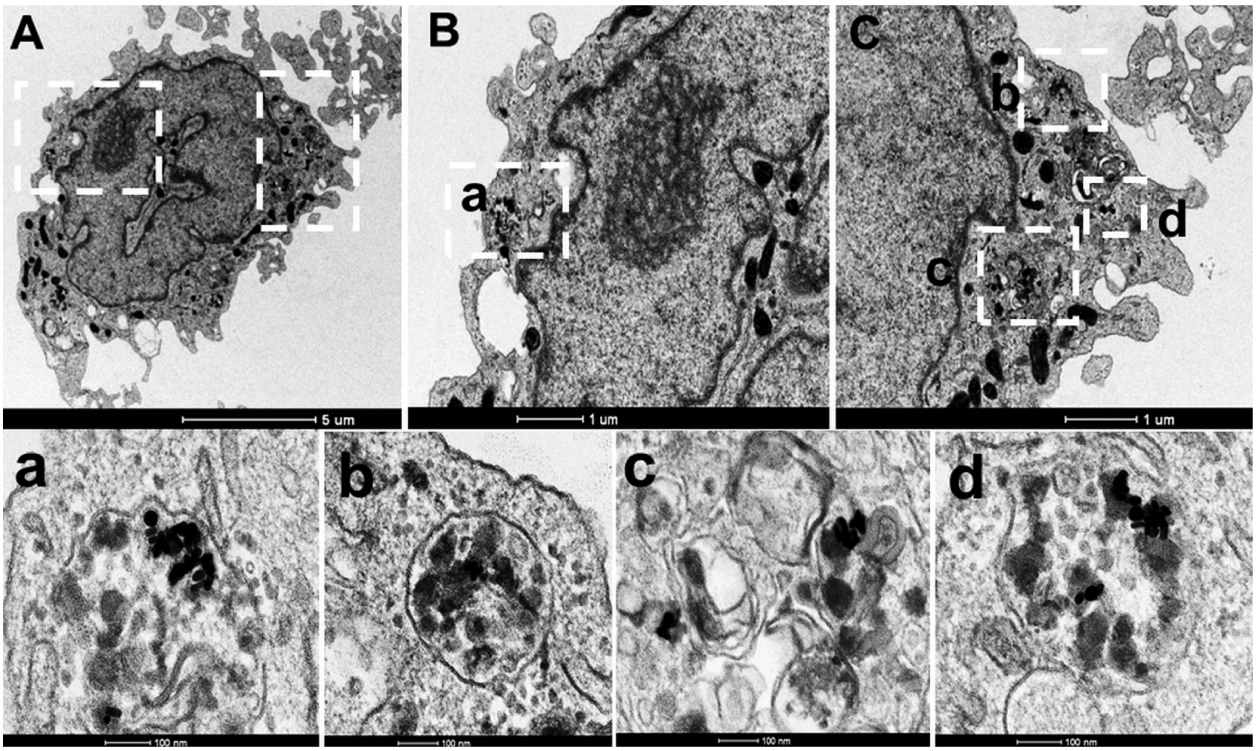

Figure 4. Cryo-TEM images of a PAH-GNRs stained M1 cell. (A) Section of the whole cell at 4.2K resolution. (B) Higher magnification (26K) of the selected areas. Further 105K magnified views of phagosomes (a−d) confirmed the presence of GNRs inside the vesicles.

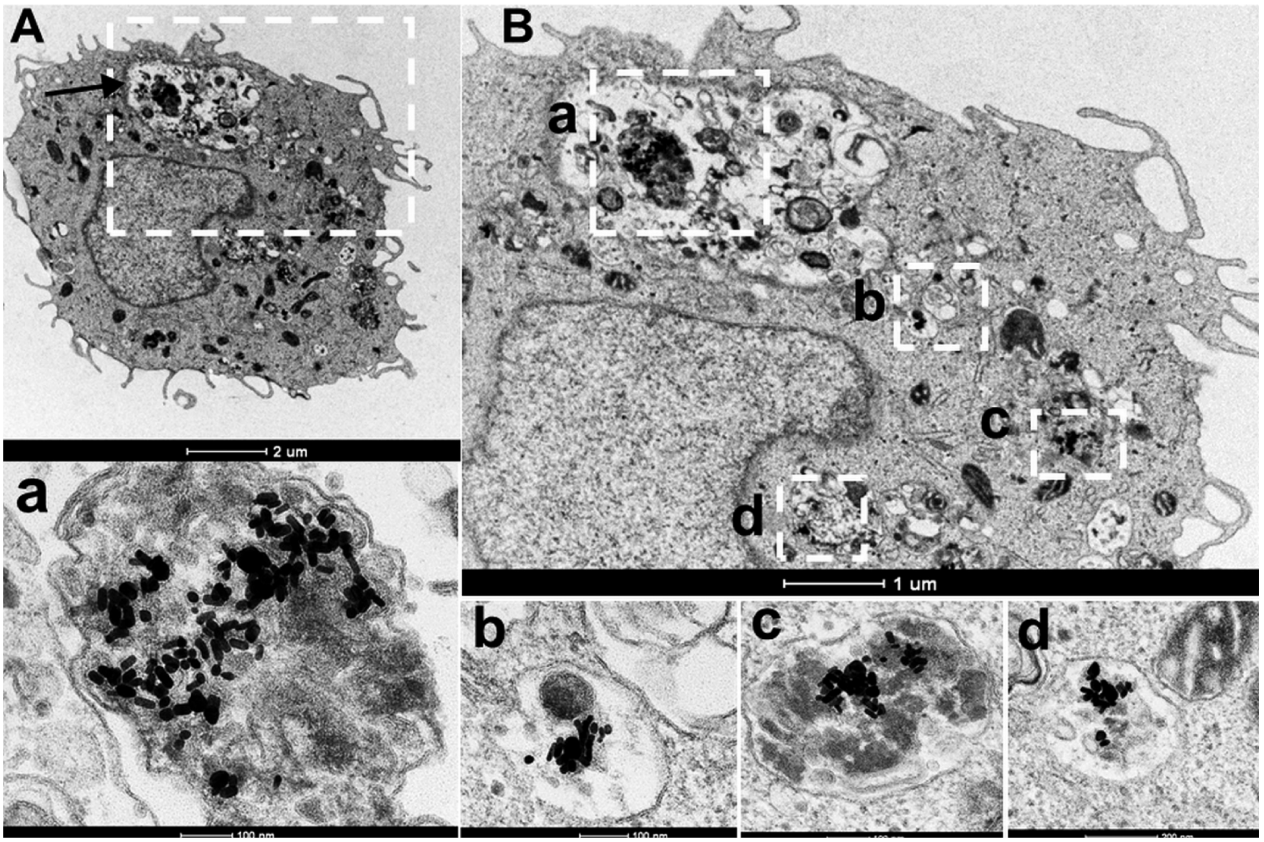

Figure 5. Cryo-TEM images of PAH-GNRs stained M2 cells. (A) Section of the whole cell at 4.2K resolution. (B) Higher magnification view (26K) of the selected areas. Further 105K magnified views of phagosomes (a−d) confirmed the presence of GNRs inside the vesicles.

accumulation is highlighted with boxes. The next panel of Figure 4B,C showed higher magnifications of the selected areas, further high-resolution images of the selected areas; panels a−d clearly depicted the presence of PAH-GNRs inside

https://dx.doi.org/10.1021/acs.nanolett.0c03525
Nano Lett. XXXX, XXX, XXX−XXX

vesicles. Mostly the GNRs were spotted inside membrane-bound vesicles and were not found in the cytoplasm, indicating their uptake through phagocytosis.

PAH-GNRs stained M2 cells showed a considerably greater number of the GNRs accumulation at the particular cellular section (Figure 5). The area of interest selected in Figure 5A gave a clear view of a large spacious phagosome along with small tight-fitting ones. An arrow points to the location of an approximately 3 μm × 1.5 μm large phagosome. Interestingly, this specious phagosome contained a distinct GNRs laden tightly fitting small phagosome with other small vesicles and apparently was in the middle of the process of fusion with lysosomes (Figure 5a). The region under panels b, c, and d further showed the presence of other small phagosomes laden with PAH-GNRs. When we compare the GNRs content between the sections of M1 and M2 cells under this study, M2 cells substantially lead. This result established real consistency with our FCM and ICP studies. Previous studies with cellular uptake of GNRs/GNS also had similar images of nanoparticle loaded vesicles. We also had performed a control set of images with M1 and M2 cells, despite GNRs (shown in Figures S27 and S28). Again, a comparison of fundamental morphology for both control and GNRs stained cells affirmed the innocuousness of GNRs. Membrane-bound empty vesicles in control cells gave a nice contrast to GNRs laden phagosomes shown here.

We then stepped toward the reason why the PAH-GNRs made a better entry into the cells. Before reaching the cellular surface, every nanoparticle has the first interaction with the biological media and, more precisely, with media organics and proteins. The formation of protein corona controls the cellular entry of nanoparticles is well documented.[44,45] In our case, the surface modification of PAH-GNRs with the media organics was far different from the other three types (Figure S29). Previous reports evidenced the effect of BSA, the major component of FBS, in the opsonization of nanoparticles. From our findings and previous experiences with different cellular events,[46,47] we also can extrapolate the fact of protein corona as the prime reason for surface modification of GNRs. Because of the negative ζ potential of BSA (−20 mV at pH 7.0), the resulted protein corona caused overall negative ζ potentials for all GNRs. With positive ζ potentials, PAH-GNRs had stronger interactions with BSA besides the other GNRs, which culminated with the larger size of the PAH-GNRs. The effect of protein corona created the advantage during phagocytosis of PAH-GNRs over PEG-, PSS-, and Cit-GNRs. We tried with NH2-PEG-GNRs to study the effect of positive change on cellular uptake (Figure S30) and ended with a mere significance in cellular uptake. More, the change in MW for PAH did not perturb their cellular intake (Figure S31). These outcomes lead us to conclude that not only the surface charge but also the protein corona of PAH-GNR made the swift entry for PAH-GNRs.

Thus, we conclude that the surface modification of PAH-GNRs helped in their cellular accumulation. On the basis of the results in this study, we believe that the higher phagocytic potency of M2 is responsible for the enhanced internalization of PAH-GNRs in M2 cells over M1, but further studies are underway to understand the exact mechanism. The differential scattering pattern of PAH-GNRs related to their cellular intake directs us to discriminate M1 and M2 cells in the flow cytometer. We are the first group to report this simple way to discriminate M1- and M2-type cells, based on the scattering profile of internalized PAH-GNRs. This is indeed remarkable progress in further cellular targeting from both *in vivo* and *in vitro* aspects. Moreover, the way of innovative application of a flow cytometer on particle-related scattering-based detection would commence a new strategy in cellular identifications. The negligible uptake of GNRs by other blood cell types affirmed the selectivity of our method toward the macrophages only. The novelty of our method lies in the future application as an *in vitro* disease detection tool just from simple tissue fluids or blood samples. This method can give easy detection of macrophages at the ailing site, which can predict the stages of manifestation of diseases like cancer, atherosclerosis, and fibrosis. We strongly believe, with further development, our method has the potency to build a new point of care or biopsy tool to facilitate early detection with a better understanding of a disease.

■ ASSOCIATED CONTENT

Supporting Information

The Supporting Information is available free of charge at https://pubs.acs.org/doi/10.1021/acs.nanolett.0c03525.

Details of the experimental section and discussion, data of characterization of GNRs, MTT viability studies, bright-field images, FCM analysis of THP1 and PBMC differentiated macrophages, FSC analysis, control TEM images, FCM data of time dependence of PAH-GNR uptake, and effect of surface polymers and media components in GNR uptake (PDF)

■ AUTHOR INFORMATION

Corresponding Author

Dror Fixler − *Faculty of Engineering and the Institute of Nanotechnology and Advanced Materials, Bar-Ilan University, Ramat-Gan 5290002, Israel;* orcid.org/0000-0003-0963-7908; Phone: 972-3-531-7598; Email: dror.fixler@biu.ac.il

Authors

Ruchira Chakraborty − *Faculty of Engineering and the Institute of Nanotechnology and Advanced Materials, Bar-Ilan University, Ramat-Gan 5290002, Israel*

Dorit Leshem-Lev − *Cardiovascular Biology Laboratories at the Felsenstein Medical Research Center and the Cardiology Department, Rabin Medical Center, Petah-Tikva 4941492, Israel*

Ran Kornowski − *Cardiovascular Biology Laboratories at the Felsenstein Medical Research Center and the Cardiology Department, Rabin Medical Center, Petah-Tikva 4941492, Israel*

Complete contact information is available at: https://pubs.acs.org/10.1021/acs.nanolett.0c03525

Author Contributions

The manuscript was written through the contributions of all authors. The experiments were performed by R.C., and D.F and D.L.-L contributed to experimental planning, data analysis, and manuscript preparation. All authors have approved the final version of the manuscript.

Notes

The authors declare no competing financial interest.

https://dx.doi.org/10.1021/acs.nanolett.0c03525
Nano Lett. XXXX, XXX, XXX−XXX

■ ACKNOWLEDGMENTS

We are indebted to the Israel Science Foundation (ISF) (1195/18) for the financial assistance of this work and the Planning and Budgeting Committee (PBC) of the Council for Higher Education of Israel for supporting R.C. with a fellowship. We thank Dr. Hagit Hauschner for her kind guidance in handling the Fortessa (BD) FACS machine.

■ REFERENCES

(1) Elhelu, M. A. The role of macrophages in immunology. *J. Natl. Med. Assoc* **1983**, *75* (3), 314−317.
(2) Gordon, S.; Martinez-Pomares, L. Physiological roles of macrophages. *Pfluegers Arch.* **2017**, *469* (3−4), 365−374.
(3) Gordon, S.; Plüddemann, A. Tissue macrophages: heterogeneity and functions. *BMC Biol.* **2017**, *15* (1), 53.
(4) Coillard, A.; Segura, E. In vivo Differentiation of Human Monocytes. *Front. Immunol.* **2019**, *10* (1907), 10:1907.
(5) Yang, J.; Zhang, L.; Yu, C.; Yang, X.-F.; Wang, H. Monocyte and macrophage differentiation: circulation inflammatory monocyte as biomarker for inflammatory diseases. *Biomark Res.* **2014**, *2* (1), 1−1.
(6) Bertani, F. R.; Mozetic, P.; Fioramonti, M.; Iuliani, M.; Ribelli, G.; Pantano, F.; Santini, D.; Tonini, G.; Trombetta, M.; Businaro, L.; Selci, S.; Rainer, A. Classification of M1/M2-polarized human macrophages by label-free hyperspectral reflectance confocal microscopy and multivariate analysis. *Sci. Rep.* **2017**, *7* (1), 8965−8965.
(7) Raggi, F.; Pelassa, S.; Pierobon, D.; Penco, F.; Gattorno, M.; Novelli, F.; Eva, A.; Varesio, L.; Giovarelli, M.; Bosco, M. C. Regulation of Human Macrophage M1-M2 Polarization Balance by Hypoxia and the Triggering Receptor Expressed on Myeloid Cells-1. *Front. Immunol.* **2017**, *8*, 1097−1097.
(8) Trombetta, A. C.; Soldano, S.; Contini, P.; Tomatis, V.; Ruaro, B.; Paolino, S.; Brizzolara, R.; Montagna, P.; Sulli, A.; Pizzorni, C.; Smith, V.; Cutolo, M. A circulating cell population showing both M1 and M2 monocyte/macrophage surface markers characterizes systemic sclerosis patients with lung involvement. *Respir. Res.* **2018**, *19* (1), 186−186.
(9) Orecchioni, M.; Ghosheh, Y.; Pramod, A. B.; Ley, K. Macrophage Polarization: Different Gene Signatures in M1(LPS+) vs. Classically and M2(LPS-) vs. Alternatively Activated Macrophages. *Front. Immunol.* **2019**, *10*, 1084−1084.
(10) Atri, C.; Guerfali, F. Z.; Laouini, D. Role of Human Macrophage Polarization in Inflammation during Infectious Diseases. *Int. J. Mol. Sci.* **2018**, *19* (6), 1801.
(11) Fairweather, D.; Cihakova, D. Alternatively activated macrophages in infection and autoimmunity. *J. Autoimmun.* **2009**, *33* (3−4), 222−230.
(12) Bobryshev, Y. V.; Ivanova, E. A.; Chistiakov, D. A.; Nikiforov, N. G.; Orekhov, A. N. Macrophages and Their Role in Atherosclerosis: Pathophysiology and Transcriptome Analysis. *BioMed Res. Int.* **2016**, *2016*, 1−13.
(13) Moore, K. J.; Sheedy, F. J.; Fisher, E. A. Macrophages in atherosclerosis: a dynamic balance. *Nat. Rev. Immunol.* **2013**, *13* (10), 709−721.
(14) Ostuni, R.; Kratochvill, F.; Murray, P. J.; Natoli, G. Macrophages and cancer: from mechanisms to therapeutic implications. *Trends Immunol.* **2015**, *36* (4), 229−239.
(15) Dandekar, R. C.; Kingaonkar, A. V.; Dhabekar, G. S. Role of macrophages in malignancy. *Ann. Maxillofac Surg* **2011**, *1* (2), 150−154.
(16) Reichel, D.; Tripathi, M.; Perez, J. M. Biological Effects of Nanoparticles on Macrophage Polarization in the Tumor Microenvironment. *Nanotheranostics* **2019**, *3* (1), 66−88.
(17) Dykman, L.; Khlebtsov, N. Gold nanoparticles in biomedical applications: recent advances and perspectives. *Chem. Soc. Rev.* **2012**, *41* (6), 2256−2282.
(18) Qin, J.; Peng, Z.; Li, B.; Ye, K.; Zhang, Y.; Yuan, F.; Yang, X.; Huang, L.; Hu, J.; Lu, X. Gold nanorods as a theranostic platform for in vitro and in vivo imaging and photothermal therapy of inflammatory macrophages. *Nanoscale* **2015**, *7* (33), 13991−14001.
(19) Murphy, C. J.; Gole, A. M.; Stone, J. W.; Sisco, P. N.; Alkilany, A. M.; Goldsmith, E. C.; Baxter, S. C. Gold Nanoparticles in Biology: Beyond Toxicity to Cellular Imaging. *Acc. Chem. Res.* **2008**, *41* (12), 1721−1730.
(20) Rane, T. D.; Armani, A. M. Two-Photon Microscopy Analysis of Gold Nanoparticle Uptake in 3D Cell Spheroids. *PLoS One* **2016**, *11* (12), e0167548−e0167548.
(21) Nguyen, V. P.; Li, Y.; Qian, W.; Liu, B.; Tian, C.; Zhang, W.; Huang, Z.; Ponduri, A.; Tarnowski, M.; Wang, X.; Paulus, Y. M. Contrast Agent Enhanced Multimodal Photoacoustic Microscopy and Optical Coherence Tomography for Imaging of Rabbit Choroidal and Retinal Vessels in vivo. *Sci. Rep.* **2019**, *9* (1), 5945−5945.
(22) Tong, L.; Wei, Q.; Wei, A.; Cheng, J.-X. Gold nanorods as contrast agents for biological imaging: optical properties, surface conjugation and photothermal effects. *Photochem. Photobiol.* **2009**, *85* (1), 21−32.
(23) Chakraborty, R.; Ankri, R.; Leshem-Lev, D.; Hochhauser, E.; Kornowski, R.; Motiei, M.; Lev, E. I.; Fixler, D. Hyperlipidemic mice as a model for a real-time in vivo detection of atherosclerosis by gold nanorods-based diffusion reflection technique. *Journal of Biophotonics* **2019**, *12* (1), No. e201800218.
(24) Ankri, R.; Duadi, H.; Motiei, M.; Fixler, D. In-vivo Tumor detection using diffusion reflection measurements of targeted gold nanorods − a quantitative study. *Journal of Biophotonics* **2012**, *5* (3), 263−273.
(25) Ankri, R.; Ashkenazy, A.; Milstein, Y.; Brami, Y.; Olshinka, A.; Goldenberg-Cohen, N.; Popovtzer, A.; Fixler, D.; Hirshberg, A. Gold Nanorods Based Air Scanning Electron Microscopy and Diffusion Reflection Imaging for Mapping Tumor Margins in Squamous Cell Carcinoma. *ACS Nano* **2016**, *10* (2), 2349−2356.
(26) Ankri, R.; Chakraborty, R.; Motiei, M.; Fixler, D. Three-Dimensional Highly Sensitive Diffusion Reflection-Based Imaging Method for the in Vivo Localization of Atherosclerosis Plaques Following Gold Nanorods Accumulation. *ACS Omega* **2018**, *3* (6), 6134−6142.
(27) Ankri, R.; Leshem-Lev, D.; Fixler, D.; Popovtzer, R.; Motiei, M.; Kornowski, R.; Hochhauser, E.; Lev, E. I. Gold Nanorods as Absorption Contrast Agents for the Noninvasive Detection of Arterial Vascular Disorders Based on Diffusion Reflection Measurements. *Nano Lett.* **2014**, *14* (5), 2681−2687.
(28) Ankri, R.; Meiri, A.; Lau, S. I.; Motiei, M.; Popovtzer, R.; Fixler, D. Intercoupling surface plasmon resonance and diffusion reflection measurements for real-time cancer detection. *Journal of Biophotonics* **2013**, *6* (2), 188−196.
(29) Fixler, D.; Ankri, R.; Kaplan, I.; Novikov, I.; Hirshberg, A. Diffusion Reflection:A Novel Method for Detection of Oral Cancer. *J. Dent. Res.* **2014**, *93* (6), 602−606.
(30) Melzer, S.; Ankri, R.; Fixler, D.; Tarnok, A. Nanoparticle uptake by macrophages in vulnerable plaques for atherosclerosis diagnosis. *Journal of Biophotonics* **2015**, *8* (11−12), 871−883.
(31) Ankri, R.; Melzer, S.; Tarnok, A.; Fixler, D. Detection of gold nanorods uptake by macrophages using scattering analyses combined with diffusion reflection measurements as a potential tool for in vivo atherosclerosis tracking. *Int. J. Nanomed.* **2015**, *10*, 4437−4446.
(32) Hu, M.; Novo, C.; Funston, A.; Wang, H.; Staleva, H.; Zou, S.; Mulvaney, P.; Xia, Y.; Hartland, G. V. Dark-field microscopy studies of single metal nanoparticles: understanding the factors that influence the linewidth of the localized surface plasmon resonance. *J. Mater. Chem.* **2008**, *18* (17), 1949−1960.
(33) Alkilany, A. M.; Nagaria, P. K.; Hexel, C. R.; Shaw, T. J.; Murphy, C. J.; Wyatt, M. D. Cellular Uptake and Cytotoxicity of Gold Nanorods: Molecular Origin of Cytotoxicity and Surface Effects. *Small* **2009**, *5* (6), 701−708.
(34) Jain, P. K.; Lee, K. S.; El-Sayed, I. H.; El-Sayed, M. A. Calculated Absorption and Scattering Properties of Gold Nanoparticles of Different Size, Shape, and Composition: Applications in

https://dx.doi.org/10.1021/acs.nanolett.0c03525
Nano Lett. XXXX, XXX, XXX−XXX

Biological Imaging and Biomedicine. *J. Phys. Chem. B* **2006**, *110* (14), 7238−7248.
(35) Ankri, R.; Fixler, D. Gold nanorods based diffusion reflection measurements: current status and perspectives for clinical applications. *Nanophotonics* **2017**, *6* (5), 1031−1042.
(36) Wu, Y.; Ali, M. R. K.; Dansby, K.; El-Sayed, M. A. Improving the Flow Cytometry-based Detection of the Cellular Uptake of Gold Nanoparticles. *Anal. Chem.* **2019**, *91* (22), 14261−14267.
(37) Zucker, R. M.; Daniel, K. M. Detection of TiO2 Nanoparticles in Cells by Flow Cytometry. *Nanoparticles in Biology and Medicine: Methods and Protocols* **2012**, 497−509.
(38) Zucker, R. M.; Daniel, K. M.; Massaro, E. J.; Karafas, S. J.; Degn, L. L.; Boyes, W. K. Detection of silver nanoparticles in cells by flow cytometry using light scatter and far-red fluorescence. *Cytometry, Part A* **2013**, *83* (10), 962−972.
(39) Gallina, M. E.; Zhou, Y.; Johnson, C. J.; Harris-Birtill, D.; Singh, M.; Zhao, H.; Ma, D.; Cass, T.; Elson, D. S. Aptamer-conjugated, fluorescent gold nanorods as potential cancer theradiagnostic agents. *Mater. Sci. Eng., C* **2016**, *59*, 324−332.
(40) Li, D.; Zhang, M.; Xu, F.; Chen, Y.; Chen, B.; Chang, Y.; Zhong, H.; Jin, H.; Huang, Y. Biomimetic albumin-modified gold nanorods for photothermo-chemotherapy and macrophage polarization modulation. *Acta Pharm. Sin. B* **2018**, *8* (1), 74−84.
(41) Xie, X.; Liao, J.; Shao, X.; Li, Q.; Lin, Y. The Effect of shape on Cellular Uptake of Gold Nanoparticles in the forms of Stars, Rods, and Triangles. *Sci. Rep.* **2017**, *7* (1), 3827.
(42) Qiu, Y.; Liu, Y.; Wang, L.; Xu, L.; Bai, R.; Ji, Y.; Wu, X.; Zhao, Y.; Li, Y.; Chen, C. Surface chemistry and aspect ratio mediated cellular uptake of Au nanorods. *Biomaterials* **2010**, *31* (30), 7606−7619.
(43) Zhu, X.-M.; Fang, C.; Jia, H.; Huang, Y.; Cheng, C. H. K.; Ko, C.-H.; Chen, Z.; Wang, J.; Wang, Y.-X. J. Cellular uptake behaviour, photothermal therapy performance, and cytotoxicity of gold nanorods with various coatings. *Nanoscale* **2014**, *6* (19), 11462−11472.
(44) Pino, P. d.; Pelaz, B.; Zhang, Q.; Maffre, P.; Nienhaus, G. U.; Parak, W. J. Protein corona formation around nanoparticles − from the past to the future. *Mater. Horiz.* **2014**, *1* (3), 301−313.
(45) Kah, J. C. Y.; Chen, J.; Zubieta, A.; Hamad-Schifferli, K. Exploiting the Protein Corona around Gold Nanorods for Loading and Triggered Release. *ACS Nano* **2012**, *6* (8), 6730−6740.
(46) Fixler, D.; Tirosh, R.; Zinman, T.; Shainberg, A.; Deutsch, M. Differential aspects in ratio measurements of [Ca2+]i relaxation in cardiomyocyte contraction following various drug treatments. *Cell Calcium* **2002**, *31* (6), 279−287.
(47) Fixler, D.; Tirosh, R.; Zurgil, N.; Deutsch, M. Tracing apoptosis and stimulation in individual cells by fluorescence intensity and anisotropy decay. *J. Biomed. Opt.* **2005**, *10* (3), 034007.

https://dx.doi.org/10.1021/acs.nanolett.0c03525
Nano Lett. XXXX, XXX, XXX−XXX